Visualizing Drug Release from a Stimuli-Responsive Soft Material Based on Amine-Thiol Displacement

Tianhong Wu,[1] Shiqing Huang,[2] Xing Feng,[1] Xiaogang Liu,[2] Tony D. James,[3,5] Xiaolong Sun*[1] and Xuhong Qian[4]

[1]The Key Laboratory of Biomedical Information Engineering of Ministry of Education, School of Life Science and Technology, Xi'an Jiaotong University, Xi'an, 710049, P. R. China.

[2]Singapore University of Technology and Design, 8 Somapah Road, 487372, Singapore.

[3]Department of Chemistry, University of Bath, Bath, BA2 7AY, UK.

[4]State Key Laboratory of Bioreactor Engineering, Shanghai Key Laboratory of Chemical Biology, School of Pharmacy, East China University of Science and Technology, Shanghai 200237, P. R. China; School of Chemistry and Molecular Engineering, East China Normal University, Shanghai 200062, P. R. China.

[5]School of Chemistry and Chemical Engineering, Henan Normal University, Xinxiang, 453007, P. R. China.

Corresponding author. Email: x.l.sun86@xjtu.edu.cn (X.L.S)

Abstract

In this research, we developed a photo luminescent platform using amine-coupled fluorophores, generated from a single conjugate acceptor containing bis-vinylogous thioesters. Based on the experimental and computational results, the fluorescence turn-on mechanism was proposed to be charge separated induced energy radiative transition for the amine-coupled fluorophore. While the sulfur containing precursor was not fluorescent since the energy internal conversion occurred through vibrational 2RS- (R represents alkyl groups) as energy acceptor(s). Further utilizing the conjugate acceptor, we establish a new fluorogenic approach via a highly cross-linked soft material to detect cysteine selectively under neutral aqueous conditions. Turn-on fluorescence emission and macroscopic degradation occurred in the presence of cysteine as the stimuli, which can be visually tracked due to the generation of an optical indicator and the cleavage of linkers within the matrix. Furthermore, a novel drug delivery system was constructed, achieving controlled release of sulfhydryl drug (6-Mercaptopurine) which was tracked by photoluminescence and high-performance liquid

chromatography. The photoluminescent molecules developed herein, are suitable for visualizing polymeric degradation making them suitable for additional "smart" material applications.

Keywords

Amine-thiol displacement induced emission, single crystal, fluorescence sensing, macromolecular degradation, drug release.

Introduction

Hydrogels are hydrophilic and biocompatible elastomers consisting of a three-dimensional network structure, consisting of a unique cross-linked matrix ensuring they exhibit soft physical properties comparable with living tissue, making them ideal biomaterials and as such they have been widely used in drug transport,[1-3] tissue engineering materials,[4-6] electrochemical devices,[7-8] as well as for other applications. Among them, stimuli-responsive degradable hydrogels are capable of undergoing changes in macroscopic morphology, mechanical properties, and other photophysical properties upon stimulation by temperature,[9] ion concentration,[10] pH,[11-12] bio-analytes,[13-14] light,[15] electricity,[16-17] or shear stress.[18-19] For this reason, numerous hydrogels have been designed to harness pathophysiology for targeted release by integrating triggered structural breakdown in response to external stimuli (e.g., enzymes, pH, temperature, redox conditions, small molecules), enabling them to respond to disease-related biochemical markers.[20-22] Up till now, the assessment of drug release and investigation of delivery efficiency have been conducted primarily through optical spectroscopy or high performance liquid chromatography (HPLC).[20-23] Among them, smart materials that use fluorescence as a sensing signal are attracting ever increasingly attention because they are more sensitive to a certain stimuli.[24-28] Furthermore, the precise structural regulation or more accurate information delivery through changing the optical properties of the material remains underdeveloped. Thus, the preparation and investigation of "intelligent" hydrogels capable of responding to a biomarker-stimuli specifically and allowing quantitative assessment of drug release through photo luminescent signals, would provide a new platform suitable for clinical diagnosis and treatment.

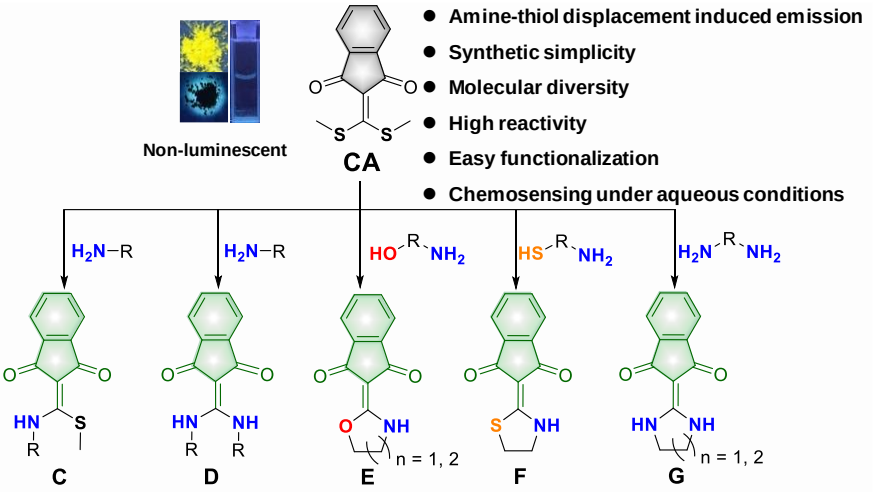

Scheme 1. General schematic of photoluminescent platform established through small molecules based coupling reactions exploited here. **CA** was the original molecule which was non-luminescence. C/D/E/F/G are the fluorophores generated through amine-thiol scrambling and cyclization with **CA**.

Previously, we developed photo luminogens which worked in an organic medium with/without catalyst or alkaline conditions, for tracking macroscopic fabrication of soft materials or chemosensing.[29-31] However, the photoluminecent mechanism remains underdeveloped, limiting additional application. With this research, we explored the indanonalkene photo luminescent platform, investigated the optical properties and proposed an optical mechanism involving amine-thiol scrambling with **CA** to generate a range of diverse fluorophores (Scheme 1). The photophysical properties were evaluated and the systems exhibited large Stokes shifts and quantum yields both in solution and solid states. Density function theory (DFT) calculations and analysis of single crystals indicated that the excited state charge separation on the amine conjugated chromophores led to the radiative decay, while **CA** with bis-vinylogous thioesters was non-fluorescent due to energy internal conversion. As such, colorimetric and fluorometric signal changes occurred for the kinetic and dose-dependent titrations between **CA** and amino thiol-containing cysteine (Cys)/homocysteine (Hcy), respectively under neutral aqueous conditions. Furthermore, we achieved fluorescent tracking of the degradation of a non-luminescent **CA**-poly(ethylene glycol) cross-linked hydrogel via chemically triggered cyclization in the presence of Cys. Moreover, a drug-loaded hydrogel system using thiol-thiol dynamic covalent bonding was developed and applied for

visualizing controlled drug release under activation by Cys, that was evaluated using cytotoxicity studies. These distinct photochemical reactions with molecular diversity, good photophysical properties, and application for the tracking of controlled drug release using stimuli-responsive soft materials could result in the development of functional materials with multiple applications.

Materials and Instruments

Materials

All chemical reagents were purchased from *Meryer, Aladdin Chemical Industry,* and *Energy Chemical,* unless otherwise noted. And used without further purification. Phosphate buffers were prepared using twice-distilled water. All cuvettes made by fused quartz were purchased from Starna Cells with standard screw and septum top. Silica gel from *Qingdaohaiyang Chemical Company* with 200-300 mesh was used for column chromatography.

Methods and instruments

Nuclear magnetic resonance (NMR)

^{1}H and ^{13}C NMR spectra were recorded on 400 MHz JEOL NMR spectrometer, Bruker Avance-400 MHz and 600 MHz NMR spectrometer. The NMR spectra were referenced to solvent and the spectroscopic solvents (chloroform-*d*, DMSO-d_6) were purchased from *Cambridge Isotope Laboratories* and *Energy Chemical.*

High-resolution mass spectrometry (HRMS)

High-resolution mass spec (HRMS) analysis was conducted by the WATERS I-Class VION IMS QTof mass spectrometer.

UV-vis spectroscopy

The UV-vis absorbance spectra and molar extinction coefficient were obtained in Cary 3500 UV-vis spectrophotometer from Agilent Technology. The spectra were run in Cary WinUV software.

Fluorescence spectroscopy

Fluorescence spectra in different solvents were measured on a HITACHI F-7100 fluorescence spectrometer. Absolute quantum yield (powder and liquid), fluorescence lifetime (powder and liquid) and fluorescence spectra of powder were measured on Edinburgh FLS980 fluorescence spectrometer. Temperature-dependent spectra were run in HORIBA FluoroMax-4 fluorescence spectrometer.

DFT calculations

DFT theoretical calculations were carried out using the Gaussian 09 program package. All the geometries of compounds were optimized at B3LYP/6-31+G(d) level. The molecular orbital (MO) plots and MO energy levels were computed at the same level of theory.

X-ray crystallography

Single crystals suitable for X-ray diffraction were obtained for ten of the compounds, **C2, D1, G2, G3** and **E2**. All data were recorded on a Bruker Apex II diffractometer, equipped with a CCD area detector and graphite-monochromated MoKα radiation (λ = 0.71073 Å) at 150 K. The structures were solved by direct methods and refined by full-matrix least-squares methods on all unique *F* values using SHELXTL. The non-hydrogen atoms were determined from different Fourier maps and refined anisotropically. CCDC 2130824, 2130826, 2130827, 2130828 and 2130856 contain the supplementary crystallographic data which can be accessed free of charge via www.ccdc.cam.ac.uk/conts/retrieving.html (or from the Cambridge Crystallographic Data Centre, 12 Union Road, Cambridge CB21EZ, UK; fax: (+44)1223-336-033; or deposit@ccdc.cam.ac.uk).

Rheological test

Rheological measurements were carried out using a Rheometer (MCR 302, Anton Paar) equipped with a parallel plate geometry (8 mm rotor). The experiments were conducted at constant temperature, i.e. 37 °C.

High performance liquid chromatography (HPLC) characterization

HPLC was performed on a Thermo Scientific™ UltiMate™ 3000 instrument (USA). HPLC method: mobile phase A (MeCN) and mobile phase B (water), flow rate: 1 mL/min, running time: 20 min, the gradient elution method: 95% to 80% B from 0 to 1 min, 80% to 20% B from 1 to 6 min. 20% B from 6 to 11 min, 20% to 80% B from 11 to 16 min, 80% to 95% B from 16 to 20 min, Detection wavelength: 320 nm. Column: Diamonsil C18(2) 5 μm 250 × 4.6 mm (Dikma). Injection volume: 20 μL.

CCK-8 cytotoxicity assays for the cell viability

The Cell Counting Kit-8 (CCK-8, purchased from mishushengwu, China) cytotoxicity assays were performed for cell viability. HepG2 cells were plated into a 96-well plate with a density of 1×10^4 per well and cultured in DMEM medium containing 10% FBS and 1% penicillin-streptomycin under standard cell culture conditions (37 °C and 5% CO_2) for 24 h. Then, the HepG2 cells were washed with fresh PBS solution, followed by addition of 100 μL supernatants of blank control, placebo control and experimental group, respectively. After four hours, HepG2 cells were further cultured with 100 μL PBS and 10 μL CCK-8 solution for another 1 h. The absorbance value was determined at 450 nm by microplate reader (Multiskan™ FC Microplate Photometer, ThermoFisher Scientific, USA). The absorbance value of cells was OD_h,

the control group was OD_c and the blank group was OD_h. The cell viability (%) = (OD_h - OD_b) / (OD_c - OD_b) * 100%.

Live/Dead staining

Live/Dead staining was conducted with HepG2 cells which were plated into a 24-well plate with a density of 1×105 per well and cultured in DMEM medium containing 10% FBS and 1% penicillin-streptomycin under standard cell culture conditions (37 °C and 5% CO_2) for 24 h. Then, the HepG2 cells were washed with fresh PBS solution, followed by addition of 100 μL supernatants of blank control, placebo control and experimental group, respectively. After four hours, the HepG2 cells were stained with 250 μL of calcein-AM/propidium iodide dye (Beyotime, China) for 30 min and observed under a fluorescent microscope (Olympus IX53 (Japan) with QIMAGING MicroPubulisher 5.0 RTV (Canada) for the green (494 nm) and red (517 nm) fluorescence.

Results and Discussion

Design and synthesis

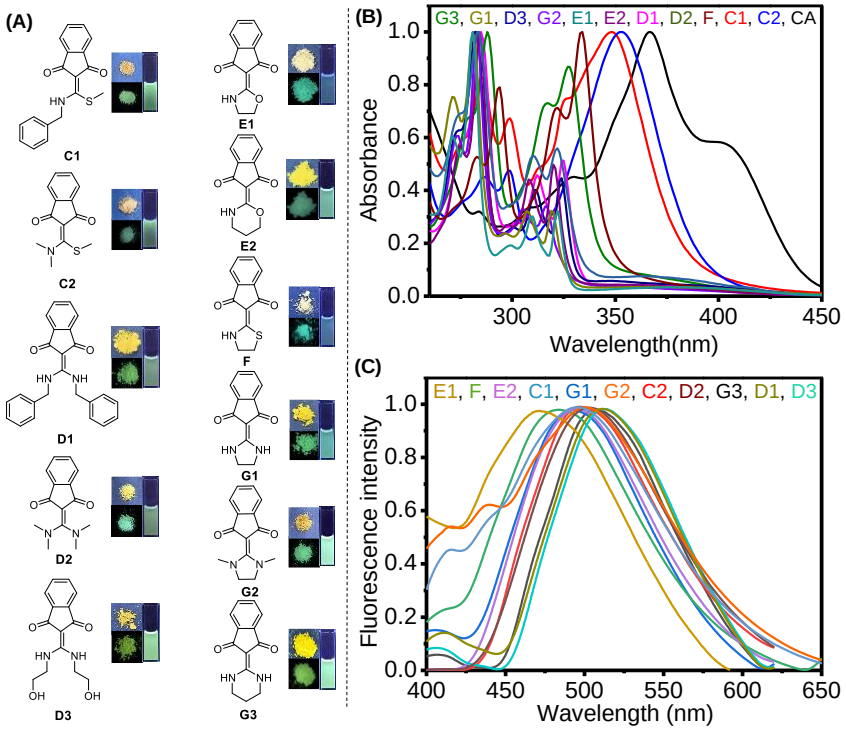

Figure 1. (A) Structures of fluorophores and images of the samples in both solution and solid states illuminated using 365 nm ultraviolet light. The medium in the cuvette was dimethylsulfoxide. (B) Normalized UV-vis and (C) Normalized fluorescence spectra of fluorophores (10 μM) and the wavelength ranges are given in Table 1 for each of the compounds.

As depicted in Scheme 1 and Figure 1, using different amine reagents, we obtained a group of fluorophores through amine-thiol scrambling and/or cyclization reaction with **CA** with concomitant release of gaseous methyl mercaptans. The products contain fluorophores with one amine attached C1-C2 or two amines attached D1-D3, *N, O*-cyclic E1-E2, *N, S*-cyclic F, *N, N*-cyclic G1-G3 (Figure 1). It should be noted that the synthesis for the compounds was like "click chemistry" with high yields (> 90%) where side-product $CH_3SH(s)$ were readily evaporated from the system which facilitated the transformation. Additionally, the synthetic process can be monitored using the fluorescence emission under a UV lamp by the naked eyes on thin layer and column chromatography, which simplified the tracking and purification. Some of the reactions could be run under aqueous conditions, indicating the efficiency of the amine-thiol and thiol-thiol coupling reactions with **CA**. More importantly, amino and sulfhydryl groups are known to be abundant in living organisms,[32] therefore these photochemical reactions could be used for potentially biological applications. The chemical structure of the products was confirmed using NMR and HRMS (see the supplementary information).

Photophysical properties for the luminophores

For the analysis of the products, their optical properties were evaluated. Firstly, it was revealed from the UV-vis absorbance spectra, that the amine-coupled luminophores, i.e., C-G displayed *ca.* λ = 14 - 86 nm blue shifts when compared with **CA** (λ_{abs} = 367 nm) (Figure 1B, Table 1), which indicated less conjugation after replacement of the thiol with an amine. In terms of fluorescence emission, the amine fluorophores exhibited turn-on fluorescence intensity and quantum yields (QY) over a range from 0.38 – 6.61% in both solid and solution states (Figure 1C, Table 1). Notably, large Stokes shifts (> 140 nm) were observed for all the fluorophores, up to 230 nm for D3 (Table 1) with two ethanolamine coupled groups. Such large Stokes shifts could be attributed to the excited-state twisted intramolecular charge transfer (TICT) process, as a strong electronic push-pull system is formed between the electron-rich amino group and the electron-deficient indandione (see below). Furthermore, the bis-amine linked fluorophore (QY for D1: 1.12%, 1.71%) exhibited higher quantum yield than the monoamine linked product (QY for C1: 0.80%, 1.00%) (Table 1). The differences confirmed that the bis-vinylogous thioesters induces fluorescence quenching of **CA** could be diminished through simple atom-atom

transformation and addition of amines. To eliminate whether the possible intramolecular proton transfer between the proton in the amino group and the carbonyl group, i.e., C1/D1, could modulate the fluorescence, we synthesized secondary amine coupled C2/D2 which all exhibited strong fluorescence and quantum yields (QY for C2: 0.78%, 0.96%; D2: 2.53%, 2.62%) in liquid and solid states, respectively (Table 1). Furthermore, the cyclic fluorophores E/F/G containing either *N,O-*/*N,S-*/*N,N-*five or six membered rings exhibited stronger photoluminescence than the corresponding non-cyclic amine fluorophores C/D in solid states (QY for E/F/G ≥ 2.92% and C/D ≤ 2.62%) (Table 1). We reasoned that the displacement of thiol(s) from the conjugate acceptor with amine(s) altered the atomic constitution and electron conjugation, resulting in absorption and fluorescence changes.

Table 1. Photophysical properties for the fluorophores

	λ_{abs}[a]	λ_{em}[a]	SS[a]	λ_{em}(solid)	ε[a, c]	Φ_F (DMSO)[d]	Φ_F (solid)[d]	τ (solid)[e]	τ (DMSO)[e]
CA	367	--[b]	--	--	2.000	--	--	--	--
C1	348	495	147	497	1.845	0.80	1.00	2.1	2.3
C2	353	500	147	489	1.834	0.78	0.96	1.1	3.8
D1	285	510	225	511	3.592	1.12	1.71	2.6	2.8
D2	288	502	214	513	2.138	2.53	2.62	4.1	2.2
D3	282	512	230	535	4.545	1.15	1.35	2.2	2.5
E1	283	482	199	482	3.884	0.38	6.61	6.7	3.0
E2	284	495	211	492	4.053	1.45	5.14	6.0	2.2
F	334	484	150	476	3.044	0.51	4.67	3.8	3.0
G1	281	495	214	514	0.954	1.29	5.49	4.5	3.1
G2	283	497	214	501	2.277	5.14	5.10	11.2	3.0
G3	281	508	227	529	4.327	1.32	2.92	2.7	2.7

[a]Spectroscopic experiments were carried out in DMSO. [b]not detected. [c]Molar extinction coefficient $\times 10^4$ L·mol^{-1}·cm^{-1}. [d]Absolute quantum yield in DMSO and solid measured using an integrating sphere. [e]Fluorescence lifetime for the molecule in solution and solid states. All steady state spectra and lifetime scans are given in Figure S2.

Proposed photoluminescence mechanism

To further elucidate the mechanism of their photoluminescence variations and confirm our speculations, the crystal structures of both the amino-coupled fluorophores and **CA** fluorophore precursor were collected and analyzed. As can be seen in Figure 2, the crystals of C2, D1, G2, G3 form *J*-aggregates (parallel dislocation stacking, the intermolecular slip angle was smaller than the critical value of 54.7°, which probably caused by the steric hindrance formed by the torsion of the alkene double bond and the interaction between the carbonyl group's lone pair of electrons and the amino group's protons combine to inhibit the formation of tight face-to-face stacking),[33] in which the strong excitonic coupling present probably affect the fluorescence of these molecules.[34-35] In addition, even the E2 crystal pairs were not parallel to each other with an angle of 11.57° between the two planes, there was almost no overlap between the pairs, which avoided intermolecular π-π interactions and thus prevented aggregation-caused quenching. Noticeably, large dihedral angles of 38.55° for C2 and 37.60° for G2, were observed due to the steric hindrance effect from methyl group(s), while the values of the other crystals were below 10°. In the case of **CA**, there was a double bond distortion with angle of 15.64°, resulting in formation of *J*-aggregates that were also non-emissive. Accordingly, both the amino-coupled fluorophore and **CA** fluorophore precursor effectively avoided π-π interaction induced quenching but exhibited different photoluminescent behavior. The fundamental question then becomes what is the structural difference and regio- or stereo-chemistry causing the difference? For **CA** which is composed of dialkyl sulfide units, free vibration and rotation of these groups might be responsible for the lack of fluorescence. While for the amine coupled fluorophore(s), vibration or rotation induced energy loss may be diminished since amine(s) as a much stronger electron donor possibly influence the conformational conjugation during photo excitation and electron density on the indanone chromophore resulting in photoluminescence change (see below).

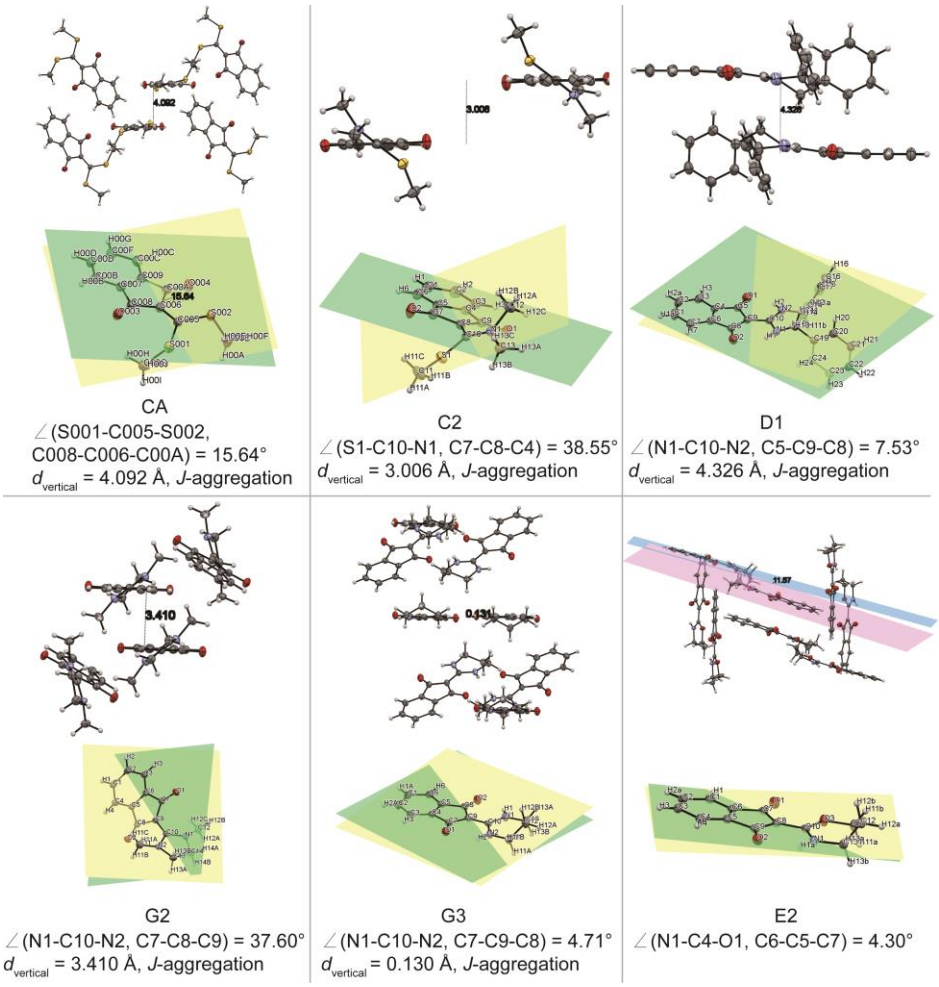

Figure 2. X-ray single crystals displaying stacking mode and single molecule. Parallel (**CA**/C2/D1/G2/G3) and non-parallel (E2) pairwise stacking mode (top) and intersecting plane angle of the alkene terminals (bottom). Data of dihedral angles, vertical distances ($d_{vertical}$) and *J*-aggregation states. Single crystals of **CA**/C2/G2/G3/E2 had been grown from dichloromethane and D1 was grown in ethanol through solvent evaporation.

Therefore, we evaluated in detail how "group displacement" was responsible for the regulation of photoluminescence. As such, we performed the spatial conformational optimization and energy level difference calculations of the HOMO-LUMO orbitals for the molecules by DFT (Figure 3A and S1). From the theoretical modeling, for the HOMO orbital of the amine derived fluorophores, the electrons are distributed over the whole molecular structure, while for the LUMO orbital, the electrons are mainly centered on the indanone part, which indicates charge separation or transfer from the double bond during the photo excitation process. For the amine coupled luminogens, the positive charge on the amine(s)

can be stabilized (Figure 3B). It was proposed that the bis-vinylogous thioesters substituents, i.e. 2RS- (R represents alky groups) resulted in excited state energy loss of **CA** most probably through free vibration or rotation, thus quenching the fluorescence through energy internal conversion after excitation.[30] The displacement of bis-vinylogous thioesters by electron-rich amino groups reduces the quenching and allows the energy from the excited state to transfer to the ground state by a radiative transition (Figure 3B). Noticeably, with two amine scrambled fluorophores D/G or replacement of one thiol with oxygen such as cyclic E, the fluorophores required higher excitation energy and emitted stronger fluorescence (Figure 3B and Table 1). The fluorophores follow the order of *N, N-* > *N, O-* > *N, S-* > *S, S-* for the excitation and emission energy pathways as depicted in the Jablonski diagram (Figure 3B). We therefore propose that the atom(s) switch or group exchange promotes the energy radiative decay of the luminogens resulting in a fluorescence emission pathway. In addition, the steric hindrance effect between spatially orientation limited methyl and carbonyl groups in G2 resulted in a large spatial distortion of the alkene double bond as mentioned above (Figure 2). Such steric repulsion resulted in G2 exhibiting better fluorescence quantum yield (>5%) amongst all the fluorophores (Table 1), which can be seen with a much larger electron separation extent with the indanone chromophore in LUMO from the DFT (Figure 3 and Figure S1).[36]

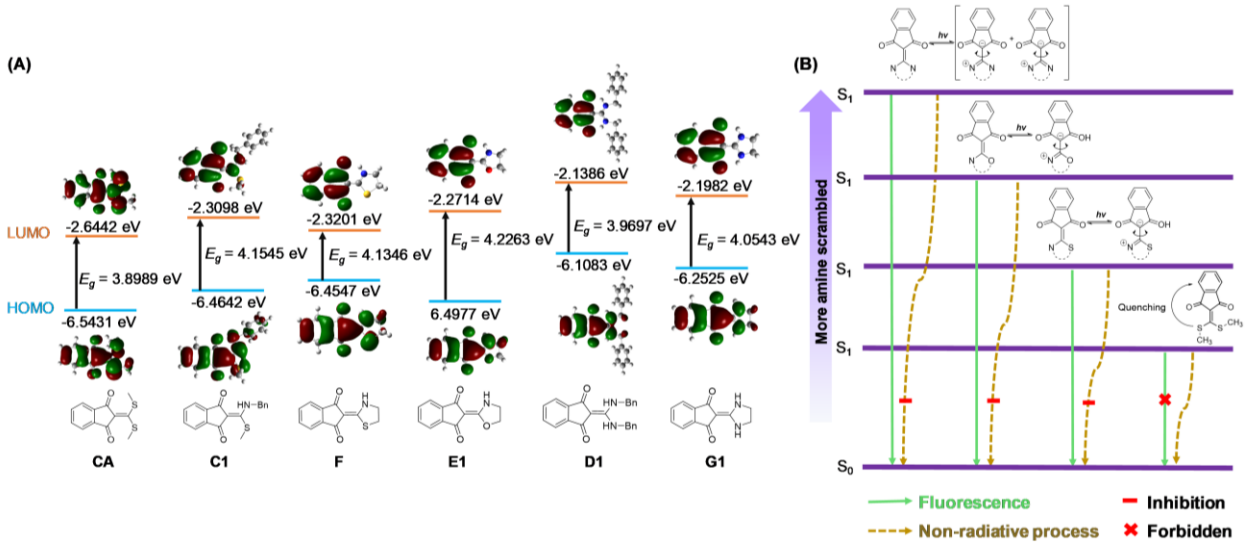

Figure 3. Proposed mechanism for the optical performance of the fluorophores. (A) DFT optimized molecular orbitals (LUMO and HOMO) of representative molecules **CA**, C1, D1, E1, F, G1. Others are given in Figure S1. All the geometries of compounds were optimized at the

B3LYP/6-31+G(d) level.[37] (B) Ground and excited states for amine-containing fluorophores and pathways for the energy radiative/non-radiative decay. Excited state charge separation and twisted states occurred on the amine molecules through electron delocalization.

Reactivity based small molecule for amino acids

Next, the reactivity of the fluorophore precursor **CA** was investigated under biological conditions towards amine thiol-containing amino acids, i.e., biomarkers Cys and Hcy. Reactions of **CA** with Cys/Hcy were carried out and the kinetics tracked in neutral aqueous buffer (Figure 4A). As the reaction proceeded, there was a regular decrease in the absorbance at λ_{abs} = 400 nm and increase at a new absorption peak λ_{abs} = 332 nm in the presence of Cys (Figure 4B, inset), while a peak at λ_{abs} = 337 nm was observed in the presence of Hcy (Figure S3A, inset), along with isosbestic point at 341 nm (For Cys, Figure 4B) and 343 nm (For Hcy, Figure S3A). A 14-fold "off-on" fluorescence enhancement at λ_{em} = 510 nm was observed for the fluorescence spectra during the reaction between **CA** and Cys over 60 min (Figure 4C). A 13-fold fluorescence enhancement at λ_{em} = 525 nm was observed for the kinetic evaluation of **CA** and Hcy (Figure S3B). Moreover, from titrations, the calibration curve of **CA** for Cys exhibited a broad concentration range (0 – 50 μM, R^2 = 0.98, Figure 4D). To verify the photochemical mechanism(s), the products generated from the reactions were confirmed using HRMS and NMR (see the supplementary information). For a mixture of **CA** (1 mM) and Cys (10 mM), the peak at m/z = 276.03269 (calcd for $C_{13}H_9NO_4S$ $[M+H]^+$ 276.03250) corresponds to compound CA-Cys (Figure S4). Pure CA-Cys and CA-Hcy products were also synthesized and characterized using NMR (Figure S5-S9). In view of the above results, we confirmed that **CA** exhibited fluorescence enhancements with Cys or Hcy (Figure S10) due to generation of five or six-heterocyclic ring systems. Since the intracellular concentration of Cys (*ca.* 200 μM) is much higher than Hcy (*ca.* 15 μM),[38] we evaluated the system with Cys further (see below).

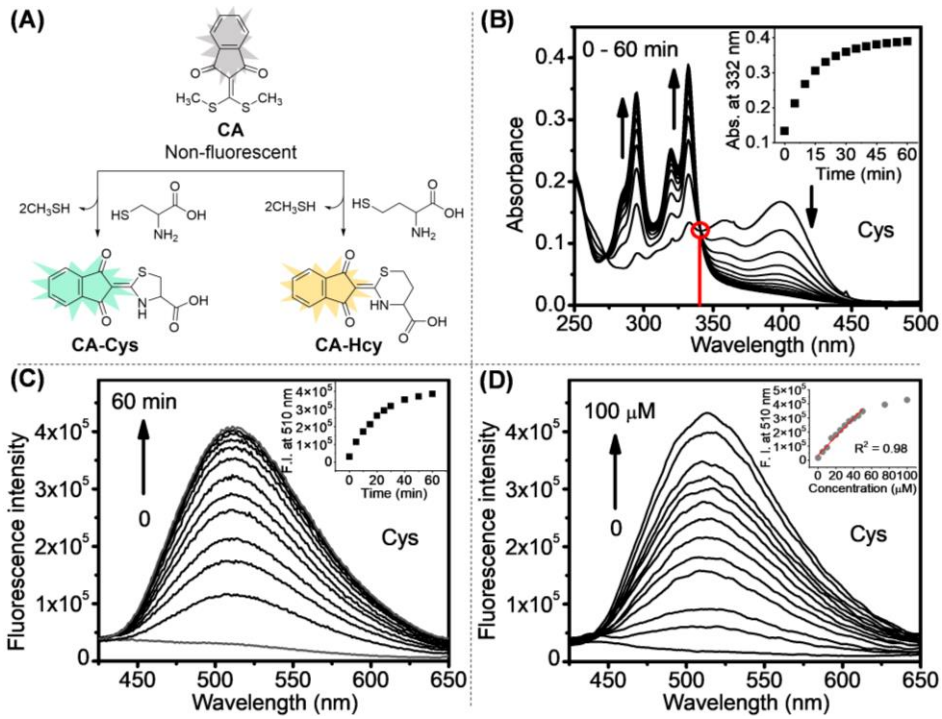

Figure 4. (A) Chemical reactions and luminescent changes of **CA** due to cyclization with Cys and Hcy, respectively under neutral aqueous conditions. (B) UV-vis spectra of of 10 μM **CA** towards 100 μM Cys as a function of time, and the relationship between the absorption at 332 nm and reaction time (inset). (C) Fluorescence spectra of 10 μM **CA** towards 100 μM Cys as a function of time, and the relationship between the fluorescence intensity at 510 nm and reaction time (inset). (D) Fluorescence spectra of 10 μM **CA** towards 0, 5, 10, 15, 20, 25, 30, 35, 40, 45, 50, 75 and 100 μM Cys, respectively, and the relationship between the fluorescence intensity at 510 nm and concentration. All spectra were determined in pH = 7.4 PBS containing 1% DMSO.

Visually tracking macromolecular degradation

The optical response of **CA** towards certain analytes led us to evaluate the stimuli-responsive properties of a soft material generated using **CA**. Thus, we synthesized a hydrogel **SM** using a CuAAC click reaction,[29, 31] highly cross-linked with the receptor within the matrix (Figure 5A) the subsequent degradation in the presence of Cys was investigated under biological conditions. The fully swelled **SM** sample (50 mg) was non-fluorescent, however, macroscopic decomposition occurred on the addition of Cys (2 mM, *ca.* 3 eq.) and fluorescence could be observed by the naked eye due to generation of the indicator CA-Cys (Figure 5A).

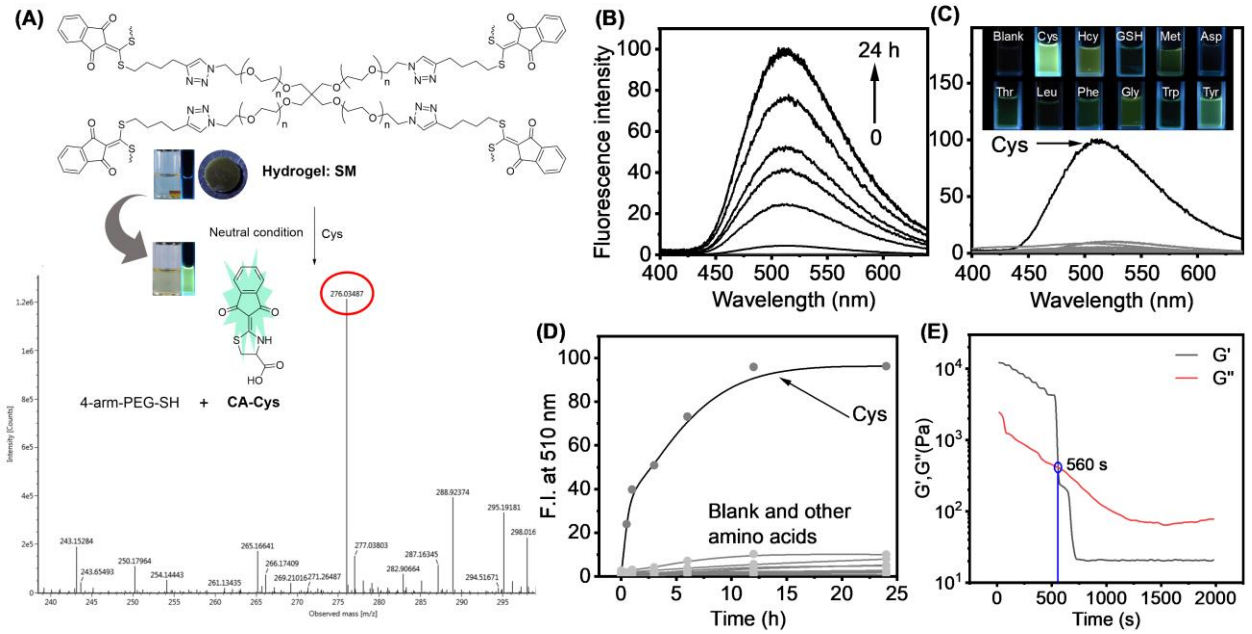

Figure 5. (A) Chemically triggered degradation of hydrogel **SM** (50 mg) and fluorescence changes resulting from Cys-induced cyclization over 0–24 h (top) and the HRMS to confirm the product (bottom). (B) Fluorescence spectra of hydrogel **SM** (50 mg) triggered by Cys (2 mM) in PBS over 0-24 h, pH = 7.4 (50% acetonitrile as co-solvent). (C) Fluorescence spectra of the degradation solution of **SM** (50 mg) after reacting with 2 mM of different amino acids for 24 h respectively in pH = 7.4 PBS (50% acetonitrile as co-solvent) (λ_{ex} = 332 nm). The fluorescence images were taken under 365 nm UV light (inset). (D)Time kinetics of fluorescence intensity at 510 nm over 24 h during **SM** degradation based on 2 mM amino acids (Hcy, GSH, Thr, Phe, Met, Gly, Leu, Asp, Trp and Tyr). (E) Rheology to monitor the degradation of hydrogel **SM** (50 mg) by Cys (5 mM) with solution point at 560 s. ω = 10 rad/s, γ = 1 %.

The optical signal changes were monitored using fluorescence spectroscopy during the degradation process, turn on fluorescence enhancement at λ_{em} = 510 nm from a solution containing CA-Cys were observed (Figure 5B). As shown in Figure 5C, selectivity experiments using the hydrogel (50 mg) exhibited a Cys-specific fluorescence response over other amino acids (Hcy, GSH, Met, Asp, Thr, Leu, Phe, Gly, Trp and Tyr). In comparison with the fluorescence images under UV light irradiation, only the solution treated with Cys exhibited strong fluorescence visible by naked eye (Figure 5C, inset). HRMS from the solution confirmed the generation of CA-Cys (Figure 5A). We also employed a rheometer to track the degradation of **SM** (50 mg) in the presence of Cys (5 mM) over time and found a solution point at 560 s with storage modulus G' lower than loss modulus G", indicating the formation of a liquid solution (Figure 5E). The

experimental results above confirmed that hydrogel **SM** exhibits good sensitivity/selectivity towards Cys, making it suitable for on-demand bio-degradation, chemosensing or controlled release.[20, 25, 39-40]

Hydrogel systems for controlled drug release

Next, we explored drug release using the degradable hydrogel. 6-Mercaptopurine (6-MP) with a free thiol was chosen since it is cell cycle specific drug that inhibit the purine synthetic pathway, and competitively inhibits the transformation of hypoxanthine, interfering with purine metabolism and impeding nucleic acid synthesis.[41] To demonstrate the suitability of our system for stimuli-responsive drug release, we prepared a sample of drug-loaded hydrogel by incorporation of 6-MP using thiol-thiol dynamic covalent bonding (Figure 6A and section 3.8 in supplementary information). Subsequently, the purified SM-drug was sterilized using alcohol immersion and UV irradiation for 60 min, respectively to obtain a sterile cell medium. Then, a sample of SM-drug (600 mg) was immersed in 5 mL Cys (5 mM, dissolved in sterile PBS), and then a portion of the supernatant (300 μL) was collected at regular intervals (5 min) and the fluorescence intensity determined, in addition to HPLC characterization of 6-MP release and a cytotoxicity assay. As shown in Figure 6B, the fluorescence intensity exhibited an 11-fold enhancement in comparison to the control group within 5 min. The 6-MP terminal release concentration was determined to be 45 μM, by evaluating the integral area ratio with free 6-MP (Retention time at 6.8 min, Figure 6C). Both the fluorescence intensity and the concentration of the 6-MP were positively correlated with the degradation time (Figure 6D). A Cell Counting Kit-8 (CCK-8) assay was then performed on HepG2 cells (human hepatocellular carcinomas) to evaluate the cell viability after 4 hours incubation with the supernatants. Significantly, the leachate at 10 min resulted in 50% cellular mortality and almost complete death after 20 min, however, normal cell viability (over 95%) was observed for the blank control group and the placebo control group (Figure 6E). Then, Live/Dead (Calcein-AM/Propidium iodide) staining were carried out to further determine the cell viability. A significant difference in red fluorescence signal (dead cells) between experimental and control groups confirmed the high efficiency of drug release by SM-drug (Figure 6F). As a positive control experiment, the Live/Dead staining of free 6-MP completely deficient in green fluorescence (live cells) (Figure S11). From all the above experiments,

it can be concluded that the high reactivity of the hydrogels towards Cys, as well as the resulting fluorescence signal can be used for the visualization of the controlled release of sulfhydryl drugs.

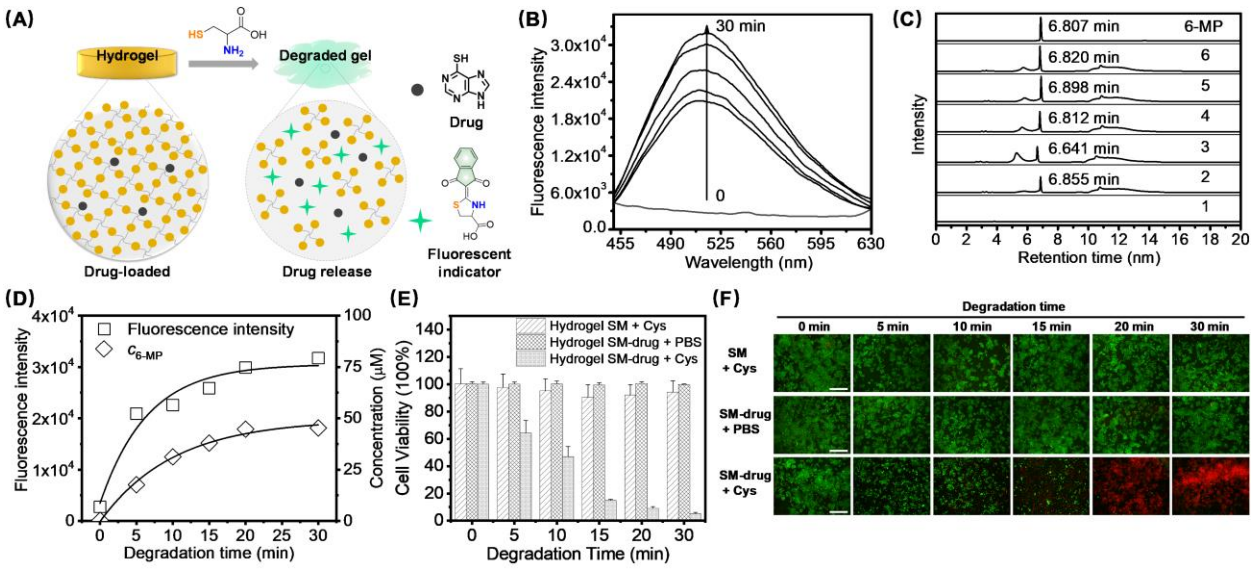

Figure 6. (A) Schematic diagram of Cys triggered hydrogel degradation, generation of indicator and drug release. (B) Fluorescence of the supernatants of SM-drug degraded by 5 mM Cys at different times. (C) HPLC spectra of supernatants in (B): sample 1-6 represent a degradation time of 0, 5, 10, 15, 20, 30 min, respectively. The chromatographic peak of the released 6-MP was located at a retention time of 6.8 min, according to the standard peak of 6-MP. (D) The relationship between fluorescence intensity at 510 nm as well as the concentration of released $C_{6\text{-MP}}$ and degradation time. (E) CCK-8 cytotoxicity assays of the supernatants of hydrogel SM and SM-drug immersed in 5 mM Cys solution or PBS with different immersion time, pH = 7.4. (F) Live/dead staining with Calcein-AM/PI of HepG2 cells pretreated by supernatants with different immersion time in 5 mM Cys solution or PBS after 4 hours, pH =7.4. Scale bar = 500 μm.

Conclusion

In summary, we have developed a general strategy for the design and development of indanonalkene fluorophores as part of photoluminescent platform via amine-thiol chemical group replacement. The amine-coupled luminogens exhibited large Stokes shift and high fluorescence quantum yields both in solid and solution states. From single crystal analysis and DFT calculations, excited state charge separation and electron delocalization by the amine was proposed to explain the photoluminescent performance, which diminished the vibrational energy loss from the bis-vinylogous thioesters on the

fluorophore precursor. The optical molecular platform exhibited good chemical sensing capacity towards thiol amine-containing amino acids while enabling the visual tracking of the degradation of a hydrogel, triggered by cysteine stimulus and cyclization under biologically appropriate conditions. Based on these observations we visually monitored the controlled release of a sulfhydryl drug from the stimuli responsive soft material. As such, our as-prepared stimuli responsive materials exhibit great promise for the construction of photoluminescent platforms and functional materials for biomedical research.

Data availability

Supporting Information is available and includes general information, general procedures for the synthesis and characterization of all compounds in this work, UV-vis / fluorescence spectra, and fluorescence images of cells.

Conflict of Interest

There is no conflict of interest to report.

Acknowledgments

XLS thanks the National Natural Science Foundation of China (No. 21907080, 22278330) and Youth Innovative Team (No. xtr052022012) from Xi'an Jiaotong University. TDJ wishes to thank the Open Research Fund of the School of Chemistry and Chemical Engineering, Henan Normal University for support (2020ZD01). We wish to thank Professor Eric V. Anslyn (UT Austin) and Amilra De Silva (Queen's University Belfast) for the discussions and suggestions.

References

1. Li, J.; Mooney, D. J., Designing Hydrogels for Controlled Drug Delivery. *Nat. Rev. Mater.* **2016,** *1* (12), 16071.
2. Oliva, N.; Conde, J.; Wang, K.; Artzi, N., Designing Hydrogels for On-Demand Therapy. *Acc. Chem. Res.* **2017,** *50* (4), 669-679.
3. Fu, X.; Hosta-Rigau, L.; Chandrawati, R.; Cui, J., Multi-Stimuli-Responsive Polymer Particles, Films, and Hydrogels for Drug Delivery. *Chem* **2018,** *4* (9), 2084-2107.
4. Griffith Linda, G.; Naughton, G., Tissue Engineering--Current Challenges and Expanding Opportunities. *Science* **2002,** *295* (5557), 1009-1014.
5. Tang, J. D.; Mura, C.; Lampe, K. J., Stimuli-Responsive, Pentapeptide, Nanofiber Hydrogel for Tissue Engineering. *J. Am. Chem. Soc.* **2019,** *141* (12), 4886-4899.

6. Zhao, Y.; Song, S.; Ren, X.; Zhang, J.; Lin, Q.; Zhao, Y., Supramolecular Adhesive Hydrogels for Tissue Engineering Applications. *Chem. Rev.* **2022,** *122,* (6), 5604–5640.
7. Wang, Z.; Tao, F.; Pan, Q., A Self-Healable Polyvinyl Alcohol-Based Hydrogel Electrolyte for Smart Electrochemical Capacitors. *J. Mater. Chem. A* **2016,** *4* (45), 17732-17739.
8. Mai, W.; Yu, Q.; Han, C.; Kang, F.; Li, B., Self-Healing Materials for Energy-Storage Devices. *Adv. Funct. Mater.* **2020,** *30* (24), 1909912.
9. Xue, Y.; Zhang, Z.; Shi, P.; Zhang, W.; Ye, Q.; Fu, D., High-Temperature Dielectric Switch and Second Harmonic Generation Integrated in A Stimulus Responsive Material. *Chin. Chem. Lett.* **2021,** *32* (1), 539-542.
10. Dong, L.; Agarwal, A. K.; Beebe, D. J.; Jiang, H., Adaptive Liquid Microlenses Activated by Stimuli-Responsive Hydrogels. *Nature* **2006,** *442* (7102), 551-554.
11. Municoy, S.; Álvarez Echazú, M. I.; Antezana, P. E.; Galdopórpora, J. M.; Olivetti, C.; Mebert, A. M.; Foglia, M. L.; Tuttolomondo, M. V.; Alvarez, G. S.; Hardy, J. G.; Desimone, M. F., Stimuli-Responsive Materials for Tissue Engineering and Drug Delivery. *Int. J. Mol. Sci.* **2020,** *21* (13).
12. Shastri, A.; McGregor, L. M.; Liu, Y.; Harris, V.; Nan, H.; Mujica, M.; Vasquez, Y.; Bhattacharya, A.; Ma, Y.; Aizenberg, M.; Kuksenok, O.; Balazs, A. C.; Aizenberg, J.; He, X., An Aptamer-Functionalized Chemomechanically Modulated Biomolecule Catch-and-Release System. *Nat. Chem.* **2015,** *7* (5), 447-454.
13. Pacifici, N.; Bolandparvaz, A.; Lewis, J. S., Stimuli-Responsive Biomaterials for Vaccines and Immunotherapeutic Applications. *Adv. Therap.* **2020,** *3* (11), 2000129.
14. Lim, J. Y. C.; Goh, S. S.; Loh, X. J., Bottom-Up Engineering of Responsive Hydrogel Materials for Molecular Detection and Biosensing. *ACS Mater. Lett.* **2020,** *2* (8), 918-950.
15. Zhang, M.; Wang, D.; Bai, B.; Wang, H.; He, L.; Li, M., The Visible Light Responsive Properties of Organogel Based on Anthracene-Substituted Acylhydrazone Derivative. *Chin. Chem. Lett.* **2018,** *29* (3), 497-500.
16. Han, D.; Farino, C.; Yang, C.; Scott, T.; Browe, D.; Choi, W.; Freeman, J. W.; Lee, H., Soft Robotic Manipulation and Locomotion with a 3D Printed Electroactive Hydrogel. *ACS Appl. Mater. Interfaces* **2018,** *10* (21), 17512-17518.
17. Liu, X.; Liu, J.; Lin, S.; Zhao, X., Hydrogel Machines. *Mater. Today* **2020,** *36,* 102-124.
18. Ma, Y.; Gao, Y.; Liu, L.; Ren, X.; Gao, G., Skin-Contactable and Antifreezing Strain Sensors Based on Bilayer Hydrogels. *Chem. Mater.* **2020,** *32* (20), 8938-8946.
19. Guo, J.; Liu, X.; Jiang, N.; Yetisen, A. K.; Yuk, H.; Yang, C.; Khademhosseini, A.; Zhao, X.; Yun, S.-H., Highly Stretchable, Strain Sensing Hydrogel Optical Fibers. *Adv. Mater.* **2016,** *28* (46), 10244-10249.
20. Badeau, B. A.; Comerford, M. P.; Arakawa, C. K.; Shadish, J. A.; DeForest, C. A., Engineered Modular Biomaterial Logic Gates for Environmentally Triggered Therapeutic Delivery. *Nat. Chem.* **2018,** *10* (3), 251-258.
21. Zhou, Q.; Hou, Y.; Zhang, L.; Wang, J.; Qiao, Y.; Guo, S.; Fan, L.; Yang, T.; Zhu, L.; Wu, H., Dual-pH Sensitive Charge-reversal Nanocomplex for Tumor-Targeted Drug Delivery with Enhanced Anticancer Activity. *Theranostics* **2017,** *7* (7), 1806-1819.
22. Yang, K.; Wan, S.; Chen, B.; Gao, W.; Chen, J.; Liu, M.; He, B.; Wu, H., Dual pH and Temperature Responsive Hydrogels Based on β-Cyclodextrin Derivatives for Atorvastatin Delivery. *Carbohydr. Polym.* **2016,** *136,* 300-306.
23. He, S.; Jacobsen, J.; Nielsen, C. U.; Genina, N.; Østergaard, J.; Mu, H., Exploration of in Vitro Drug Release Testing Methods for Saquinavir Microenvironmental pH Modifying Buccal Films. *Eur. J. Pharm. Sci.* **2021,** *163,* 105867.
24. Cai, L.; Xiong, X.; Qiao, M.; Guo, J.; Zhang, H.; Lin, J.; Liu, S.; Jia, Y.-G., Aggregation-Induced Emission Luminogen Based Self-Healing Hydrogels Fluorescent Sensors for α-Amylase. *Polym. Chem.* **2022,** *13* (6), 819-828.
25. Zhou, Q.; Dong, X.; Xiong, Y.; Zhang, B.; Lu, S.; Wang, Q.; Liao, Y.; Yang, Y.; Wang, H., Multi-Responsive Lanthanide-Based Hydrogel with Encryption, Naked Eye Sensing, Shape Memory, Self-Healing, and Antibacterial Activity. *ACS Appl. Mater. Interfaces* **2020,** *12* (25), 28539-28549.
26. Qiu, H.; Wei, S.; Liu, H.; Zhan, B.; Yan, H.; Lu, W.; Zhang, J.; Wu, S.; Chen, T., Programming Multistate Aggregation-Induced Emissive Polymeric Hydrogel into 3D Structures for On-Demand Information Decryption and Transmission. *Adv. Intell. Syst.* **2021,** *3* (6), 2000239.
27. Liu, H.; Wei, S.; Qiu, H.; Si, M.; Lin, G.; Lei, Z.; Lu, W.; Zhou, L.; Chen, T., Supramolecular Hydrogel with Orthogonally Responsive R/G/B Fluorophores Enables Multi-Color Switchable Biomimetic Soft Skins. *Adv. Funct. Mater.* **2022,** *32* (9), 2108830.
28. Li, B.; Ding, Z.-J.; Li, Z.; Li, H., Simultaneous Enhancement of Mechanical Strength and Luminescence Performance

in Double-Network Supramolecular Hydrogels. *J. Mater. Chem. C* **2018,** *6* (25), 6869-6874.
29. Wu, T.; Feng, X.; Sun, X., Chemically Triggered Soft Material Macroscopic Degradation and Fluorescence Detection Using Self-Propagating Thiol-Initiated Cascades. *Polym. Chem.* **2022,** *13* (7), 922-928.
30. Wu, T.; Bian, W.; Wang, C.; Qiu, J.; Sun, X.; Qian, X., A Ring-Controlled Fluorescent Platform for Visualizing Polymer Degradation. *Aggregate* **2022,** *00,* e295. https://doi.org/10.1002/agt2.295.
31. Feng, X.; Wu, T.; Sun, X.; Qian, X., "Indanonalkene" Photoluminescence Platform: Application in Real-Time Tracking the Synthesis, Remodeling, and Degradation of Soft Materials. *J. Am. Chem. Soc.* **2021,** *143* (51), 21622-21629.
32. Brosnan, J. T.; Brosnan, M. E., The Sulfur-Containing Amino Acids: An Overview. *J. Nut.* **2006,** *136* (6), 1636S-1640S.
33. Ma, X.; Huang, Y.; Chen, W.; Liu, J.; Liu, S. H.; Yin, J.; Yang, G.-F., J-Aggregates Formed by NaCl Treatment of Aza-Coating Heptamethine Cyanines and Their Application to Monitoring Salt Stress of Plants and Promoting Photothermal Therapy of Tumors. *Angew. Chem. Int. Ed.* **2023,** *62* (3), e202216109.
34. Peng, Q.; Shuai, Z., Molecular Mechanism of Aggregation-Induced Emission. *Aggregate* **2021**, *2,* e91.
35. Wurthner, F.; Kaiser, T. E.; Saha-Moller, C. R., J-Aggregates: from Serendipitous Discovery to Supramolecular Engineering of Functional Dye Materials. *Angew. Chem. Int. Ed. Engl.* **2011,** *50* (15), 3376-410.
36. Wang, C.; Chi, W.; Qiao, Q.; Tan, D.; Xu, Z.; Liu, X., Twisted Intramolecular Charge Transfer (TICT) and Twists Beyond TICT: from Mechanisms to Rational Designs of Bright and Sensitive Fluorophores. *Chem. Soc. Rev.* **2021,** *50* (22), 12656-12678.
37. Frisch, M. J.; Trucks, G. W.; Schlegel, H. B.; Scuseria, G. E.; Robb, M. A.; Cheeseman, J. R.; Scalmani, G.; Barone, V.; Petersson, G. A.; Nakatsuji, H.; Li, X.; Caricato, M.; Marenich, A. V.; Bloino, J.; Janesko, B. G.; Gomperts, R.; Mennucci, B.; Hratchian, H. P.; Ortiz, J. V.; Izmaylov, A. F.; Sonnenberg, J. L.; Williams; Ding, F.; Lipparini, F.; Egidi, F.; Goings, J.; Peng, B.; Petrone, A.; Henderson, T.; Ranasinghe, D.; Zakrzewski, V. G.; Gao, J.; Rega, N.; Zheng, G.; Liang, W.; Hada, M.; Ehara, M.; Toyota, K.; Fukuda, R.; Hasegawa, J.; Ishida, M.; Nakajima, T.; Honda, Y.; Kitao, O.; Nakai, H.; Vreven, T.; Throssell, K.; Montgomery Jr., J. A.; Peralta, J. E.; Ogliaro, F.; Bearpark, M. J.; Heyd, J. J.; Brothers, E. N.; Kudin, K. N.; Staroverov, V. N.; Keith, T. A.; Kobayashi, R.; Normand, J.; Raghavachari, K.; Rendell, A. P.; Burant, J. C.; Iyengar, S. S.; Tomasi, J.; Cossi, M.; Millam, J. M.; Klene, M.; Adamo, C.; Cammi, R.; Ochterski, J. W.; Martin, R. L.; Morokuma, K.; Farkas, O.; Foresman, J. B.; Fox, D. J. *Gaussian 16 Rev. C.01,* Wallingford, CT, 2016.
38. Guo, T.; Chen, X.; Qu, W.; Yang, B.; Tian, R.; Geng, Z.; Wang, Z., Red and Near-Infrared Fluorescent Probe for Distinguishing Cysteine and Homocysteine through Single-Wavelength Excitation with Distinctly Dual Emissions. *Anal. Chem.* **2022,** *94* (12), 5006-5013.
39. Carberry, B. J.; Hernandez, J. J.; Dobson, A.; Bowman, C. N.; Anseth, K. S., Kinetic Analysis of Degradation in Thioester Cross-linked Hydrogels as a Function of Thiol Concentration, pKa, and Presentation. *Macromolecules* **2022,** *55* (6), 2123-2129.
40. Nguyen, M. K.; Huynh, C. T.; Gilewski, A.; Wilner, S. E.; Maier, K. E.; Kwon, N.; Levy, M.; Alsberg, E., Covalently Tethering siRNA to Hydrogels for Localized, Controlled Release and Gene Silencing. *Sci. Adv.* **2019,** *5* (8), eaax0801.
41. Karran, P.; Attard, N., Thiopurines in Current Medical Practice: Molecular Mechanisms and Contributions to Therapy-Related Cancer. *Nat. Rev. Cancer* **2008,** *8* (1), 24-36.

Table of Contents Graphic

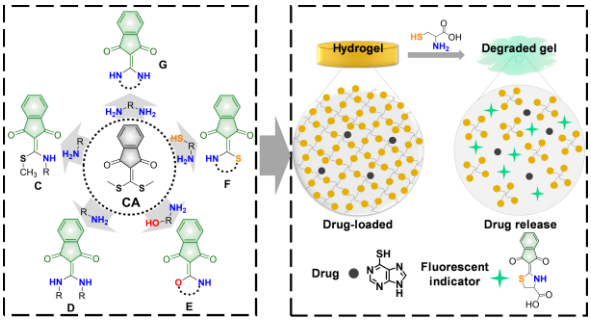

A series of benzene-based heterocyclic fluorophores were used as a photoluminescent platform. The chemical reactivity and photophysical characteristics were then applied in chemosensing and for visualizing drug release from a stimuli-responsive soft material.